

Near-IR imaging towards a puzzling YSO precessing jet

S. Paron^{1,2}, C. Fariña³, and M. E. Ortega¹

¹ Instituto de Astronomía y Física del Espacio (IAFE), CC 67, Suc. 28, 1428 Buenos Aires, Argentina
e-mail: sparon@iafe.uba.ar, mortega@iafe.uba.ar

² CBC and FADU - Universidad de Buenos Aires, Ciudad Universitaria, Buenos Aires, Argentina

³ Isaac Newton Group of Telescopes, E-38700, La Palma, Spain
e-mail: cf@ing.iac.es

Received <date>; Accepted <date>

ABSTRACT

Aims. The study of jets related to stellar objects in formation is important because it enables us to understand the history of how the stars have built up their mass. At present there are many studies concerning jets towards low-mass young stellar objects, while equivalent studies towards massive or intermediate-mass young stellar objects are scarce. In a previous study, based on ¹²CO J=3–2 and public near-IR data, we found highly misaligned molecular outflows towards the infrared point source UGPS J185808.46+010041.8 (IRS along this work), and some infrared features suggesting the existence of a precessing jet.

Methods. Using near-infrared data acquired with Gemini-NIRI at the *JHKs*-broad-bands and narrow-bands centered at the emission lines of [FeII], H₂ 1-0 S(1), H₂ 2-1 S(1), Brγ, and CO 2-0 (bh), we studied the circumstellar environment of IRS with an angular resolution between 0′′35 and 0′′45.

Results. The emission in the *JHKs*-broad-bands shows, with great detail, the presence of a cone-like shape nebula extending to the north/northeast of the point source, which appears to be attached to it by a jet-like structure. In the three bands the nebula is resolved in a twisted-shaped feature composed by two arc-like features and a bow shock-like structure seen mainly in the *Ks*-band, which strongly suggests the presence of a precessing jet. An analysis of proper motions based on our Gemini observations and UKIDSS data gives additional support to the precession scenario. We are presenting one of the best resolved cone-like nebula likely related to a precessing jet up to date. The analysis of the observed near-infrared lines shows that the H₂ is collisionally excited, and the spatial coincidence of the [FeII] and H₂ emissions in the closer arc-like feature suggests that this region is affected by a J-shock. The second arc-like feature presents H₂ emission without [FeII] which suggests the presence of a nondissociative C-shock or a less energetic J-shock. The H₂ 1-0 S(1) continuum subtracted image, reveals several knots and filaments at a larger spatial scale around IRS, in perfect matching with the distribution of the red and blueshifted molecular outflows discovered in our previous work. A not resolved system of YSOs is suggested to explain the distribution of the analyzed near-infrared features and the molecular outflows, which in turns explain the jet precession through tidal interactions.

Key words. Stars: formation – Stars: protostars – ISM: jets and outflows

1. Introduction

From observations and theoretical studies it is known that when a star forms, jets arise from a region in close proximity to the accreting source, which extract mass and angular momentum from the underlying disk. The study of jets related to stellar objects in formation enables us to understand the history of how the stars have built up their mass. As the jets penetrate their surroundings, they transfer momentum and accelerate matter, generating the ubiquitous molecular outflows commonly found in the surroundings of young stellar objects (YSOs) (Reipurth & Bally 2001; McKee & Ostriker 2007). Outflow (a)symmetries provide information about the dynamical environment of the engine and the interstellar medium in which they spread; the so called S- and Z-shaped symmetries indicate that the outflow axis has changed over time, probably due to precession induced by a companion, or interactions with sibling stars in a cluster (Bally et al. 2007), while C-shaped bends may indicate motion of surrounding gas or motion of the outflow source itself. More recently, it has been suggested that the jet precession may be produced also by the misalignment between the protostar ro-

tation axis and the magnetic fields (Ciardi & Hennebelle 2010; Lewis et al. 2015). At present there are many studies concerning the (a)symmetries of jets and outflows, mainly towards the Orion and Carina Nebula, which are very rich in HH objects related to low-mass YSOs (e.g. Lefloch et al. 2007; Bally et al. 2009, 2012; Davis et al. 2011; Reiter et al. 2015). However, equivalent studies towards massive or intermediate-mass YSOs are less common (e.g. Preibisch et al. 2003; Weigelt et al. 2006; Paron et al. 2013). Factors as the complexity of the environments, stellar multiplicity, and scarceness of massive YSOs in our proximity, make the observational studies towards these objects both, challenging and encouraging.

In a previous paper (Paron et al. 2014; hereafter Paper I) we presented results from the observation of highly misaligned molecular outflows towards the infrared (IR) point source UGPS J185808.46+010041.8 (Lucas et al. 2008; Ukidss 2012). Analyzing public UKIDSS near-IR data (*JHKs* broad-bands) extracted from the WFCAM Science Archive we found some diffuse emission showing a cone-like nebula related to the point source, which could be due to a cavity cleared in the circumstellar material by a precessing jet. This source, located at a distance of about 1.1 kpc (Lumsden et al. 2013), was suggested

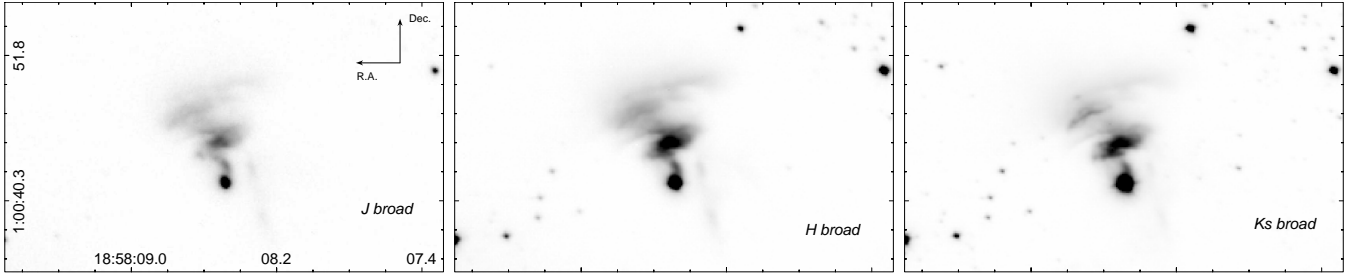


Fig. 1. *JHKs* broad-bands emission.

to be a young intermediate-mass protostar (about $3 M_{\odot}$) from an spectral energy distribution (SED) analysis (Paper I).

In order to study the origins of the misalignment of the molecular outflows and the possibility of a precessing jet, we obtained high-resolution images of this source with NIRC2, at the Gemini Telescope, using a set of broad- and narrow-band near-IR filters.

2. Observations and data reduction

In this study we analyze several near-IR broad- and narrow-band images (see Table 1) towards the source UGPS J185808.46+010041.8 (hereafter IRS). The images were acquired with NIRC2, Near InfraRed Imager and Spectrometer (Hodapp et al. 2003) at Gemini-North 8.2-m telescope. The observations were carried out during August and October 2014, and April 2015 in queue mode (Band-1 Program GN-2014B-Q-35). NIRC2 was used with the f/6 camera that provides a plate scale of $0''.117 \text{ pix}^{-1}$ in a field of view of $120'' \times 120''$.

To optimize telescope time the images were performed following a dither pattern in which the offsets directions and amplitudes were selected to be able to perform the near-IR background correction using the on-source images. For the dither pattern, particular careful was taken to avoid the contamination on the IRS source and its associated nebular emission by a saturated field star, located at about 30 arcsec from the IRS source, which residuals inevitably remain in subsequent images.

For data reduction NIRC2 images were firstly passed through *nirc2.py*, a Python script provided by the Gemini Observatory that applies a per-pixel linearity correction. All subsequent processes as background correction, images co-addition, and astrometric solution were performed with Theli (Schirmer 2013; Erben et al. 2005). For the absolute astrometric solution, stars in the field from the 2MASS 6X Point Source Working Database Catalog (Cutri et al. 2012) were used.

Table 1 lists the filters used with their central wavelength and width, the effective spatial resolution measured as the average FWHM of point sources in the final co-added images, the number of individual frames, and the effective exposure times of the final co-added images. All images were later normalized to 1 sec.

The *H*-cont image was used to subtract the continuum of [FeII] while the *K*-cont one to subtract the continuum of H_2 1-0 S(1), Br γ , H_2 2-1 S(1), and CO 2-0 (bh). For the continuum subtraction the images were convolved with an elliptical Gaussian function using the *gauss* IRAF¹ task to achieve a similar PSF for the point sources at the central area of both images. In this process the effective resolution of both images was degraded

Table 1. Near-IR bands observed with NIRC2 at Gemini-North.

Filter	λ_c (μm)	Width (μm)	Eff. Resol. (arcsec)	Frames	Exp. Time (sec)
<i>Broad-bands</i>					
<i>J</i>	1.25	0.18	0.37	19	343.90
<i>H</i>	1.65	0.29	0.4	19	68.4
<i>Ks</i>	2.15	0.35	0.34	14	15.4
<i>Narrow-bands</i>					
<i>H</i> -cont	1.570	0.0236	0.42	44	1764.40
[FeII]	1.644	0.0387	0.38	44	1764.40
<i>K</i> -cont	2.0975	0.0275	0.42	16	129.60
H_2 1-0 S(1)	2.2139	0.0261	0.44	27	218.70
Br γ	2.1686	0.0295	0.40	24	194.40
H_2 2-1 S(1)	2.2465	0.0301	0.38	27	218.70
CO 2-0 (bh)	2.289	0.0279	0.36	29	234.90

to a similar value. After convolution the images were scaled to account for the differences in filter width and throughput, and other effects derived from observing conditions in different nights (both instrumental and environmental). An initial scale factor was derived from aperture photometry of point sources in the central part of the field, this value was checked to be in agreement with the values derived from the ratio of filters transmissions. The initial scale factors were later fine-tuned by visual inspection of the residuals in subtracted images. The object nebular emission in all the subtracted images is above 5σ over the background.

3. Results

Figure 1 displays, in three panels, the emission of the *JHKs* broad-bands obtained towards IRS. It can be appreciated, with great detail, the presence of a nebula extending to the north/northeast of the point source, which appears to be attached to IRS by a jet-like structure. The nebula is mainly composed by two arc-like features, the closer to the source is more intense than the farther one, which is more extended and diffuse. In the three bands the nebula connected with the jet-like structure is resolved in a twisted-shaped feature. Besides, the emission at the *Ks*-band presents a noteworthy bow shock-like structure to the northeast. Figure 2 displays in a three-colour image the *JHKs* bands where the mentioned structures on the three bands can be appreciated superimposed. It is worth noting that these images improve, in resolution and sensitivity, the *JHKs* images from UKIDSS presented in Paper I, being one of the best near-IR images set obtained towards this kind of nebularities related to intermediate/high-mass YSOs presented up to date.

¹ IRAF is distributed by the NOAO, which are operated by the AURA, Inc., under cooperative agreement with the NSF.

Figure 3 presents the continuum emission at the observed narrow-bands H and K_s , while Fig. 4 displays the narrow-band images, centered at the emission lines of [FeII], H_2 1-0 S(1), H_2 2-1 S(1), Br γ , and CO 2-0 (bh), with and without continuum (left and right panels, respectively). As expected, the images of the narrow-band filters with the continuum shows diffuse emission with similar morphology as the observed in the broad-band images, whereas some features and knots likely due to the pure line emission are more evident in the narrow-band images. Analyzing the continuum subtracted images it can be appreciated that the [FeII] emission shows two bright knots at the end of the jet-like structure that extends from the stellar source to the closer arc-like feature. These knots are located at the projected distance of 2.8 and 1.7 arcsecs from IRS (~ 0.015 and 0.009 pc, respectively at the assumed distance of 1.1 kpc). In the close surroundings of IRS, the H_2 1-0 S(1) line shows several knots located at different distances, most of them lying at the arc-like feature closer to IRS (located at the projected distance of about 3.2 arcsecs, i.e. ~ 0.017 pc from IRS), then a bow shock feature composed by two arc-like structures at a projected distance of 5.5 arcsecs (~ 0.03 pc) from IRS, and finally an isolated and farthest knot towards the northeast at a projected distance of 7.4 arcsecs (~ 0.04 pc) from the stellar source. The morphology of the H_2 2-1 S(1) emission resembles to that of the lower transition, presenting the same features in the close surroundings of IRS, but fainter. The CO 2-0 (bh) line shows diffuse emission composed by two structures located at the arc-like feature closer to IRS, although these structures has to be taken with caution as the CO 2-0 (bh) emission shape was sensitive to the parameters chosen for the continuum subtraction. Finally, the Br γ presents also some diffuse emission with a peak slightly shifted with respect the westernmost CO structure.

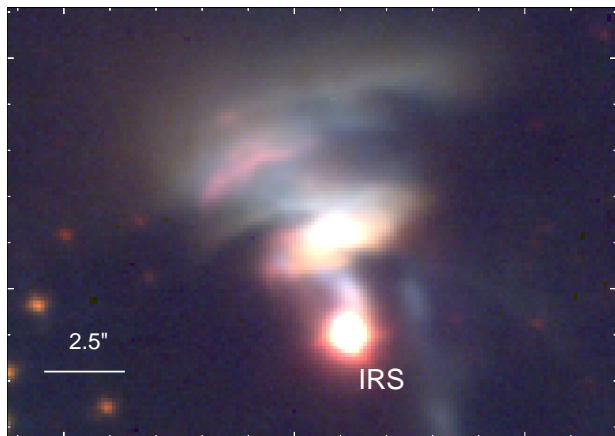


Fig. 2. Three-colour image with the $JHKs$ broad-bands emission presented in blue, green, and red, respectively.

To compare the emission-line features along the cone-like shape nebulosity, we perform a similar analysis as done in Davis et al. (2011). In Fig. 5 we present the profiles of [FeII], H_2 1-0 and 2-1 S(1) (top panel), and CO 2-0 (bh) and Br γ (bottom panel). In both plots the continuum emission in the K -band, observed with the K -cont filter, is included for comparison. These profiles were generated by integrating the emissions along a line perpendicular to the cone axis across the whole extension of the cone-like shape nebulosity. As the H_2 1-0 S(1) extends in knots and filaments much further than the other emission lines (see below), for its profile plot we have only included the emission found in the close surroundings of IRS. Table 2 shows the peak

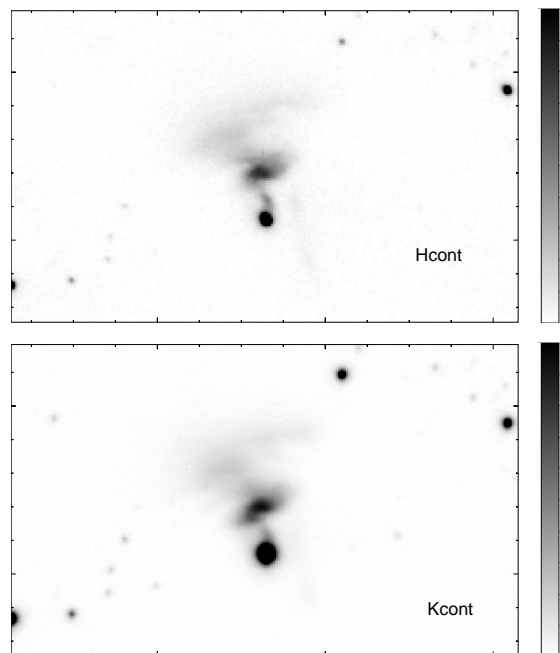


Fig. 3. Narrow-bands H - and K -continuum in upper and bottom panels, respectively. The white and black in the colorbars represent 0% and 100% of emission, and the maximum values are 3 and 30 ADU for the H - and K -cont emission, respectively. All images were normalized to 1 sec.

positions of each observed feature obtained from Gaussian fits to the profiles presented in Fig. 5. The errors from the Gaussian fits are about 10%, which in most of the cases are values smaller than the effective spatial resolution of the observations.

From this analysis it can be appreciated that the emission lines profiles (except the H_2 1-0 S(1)) peak with the highest intensity at the position of the IRS source. In similar way, all the emission lines have a second peak between 2 and 3 arcsec offset. There is a third peak of emission at about 6 arcsec offset but only for H_2 1-0 S(1) and H_2 2-1 S(1). These last two emission peaks are generated by the two arc-like features clearly displayed in the 2-D images. An inspection of the 2-D images shows that the second peak in the [FeII] profile is generated by projected blend of the profiles of more ‘compact knots’ (in contrast with the more diffuse nebula of Br γ and H_2 lines). As mentioned before, both H_2 emission lines, that trace regions of low-excitation, extend beyond being interesting to note here the case of H_2 1-0 S(1), for which the projected emission increases with the distance to the source. It is important to note that any comparison with the equivalent analysis presented in Davis et al. (2011) should be done with care because both studies are applied to sources of different mass, as in the mentioned work the study is on Herbig-Haro type outflow sources.

In order to study the excitation conditions of the H_2 lines we perform the intensity ratio between the H_2 S(1) 1-0 and H_2 S(1) 2-1 lines towards the three H_2 structures defined in Fig. 5, whose offset on the sky from IRS are shown Table 2. The obtained values are about 10 for the first arc-like feature (first peak of the H_2 profiles in Fig. 5), and ~ 25 for the second arc-like feature (second peak in Fig. 5) and for the isolated and farthest knot (third tiny peak in the same figure). In Sec. 4.1 we discuss these.

Finally, we have carefully inspected the images looking for emission likely related to IRS at larger spatial scales. The only case in which emission extends beyond the localized in the IRS

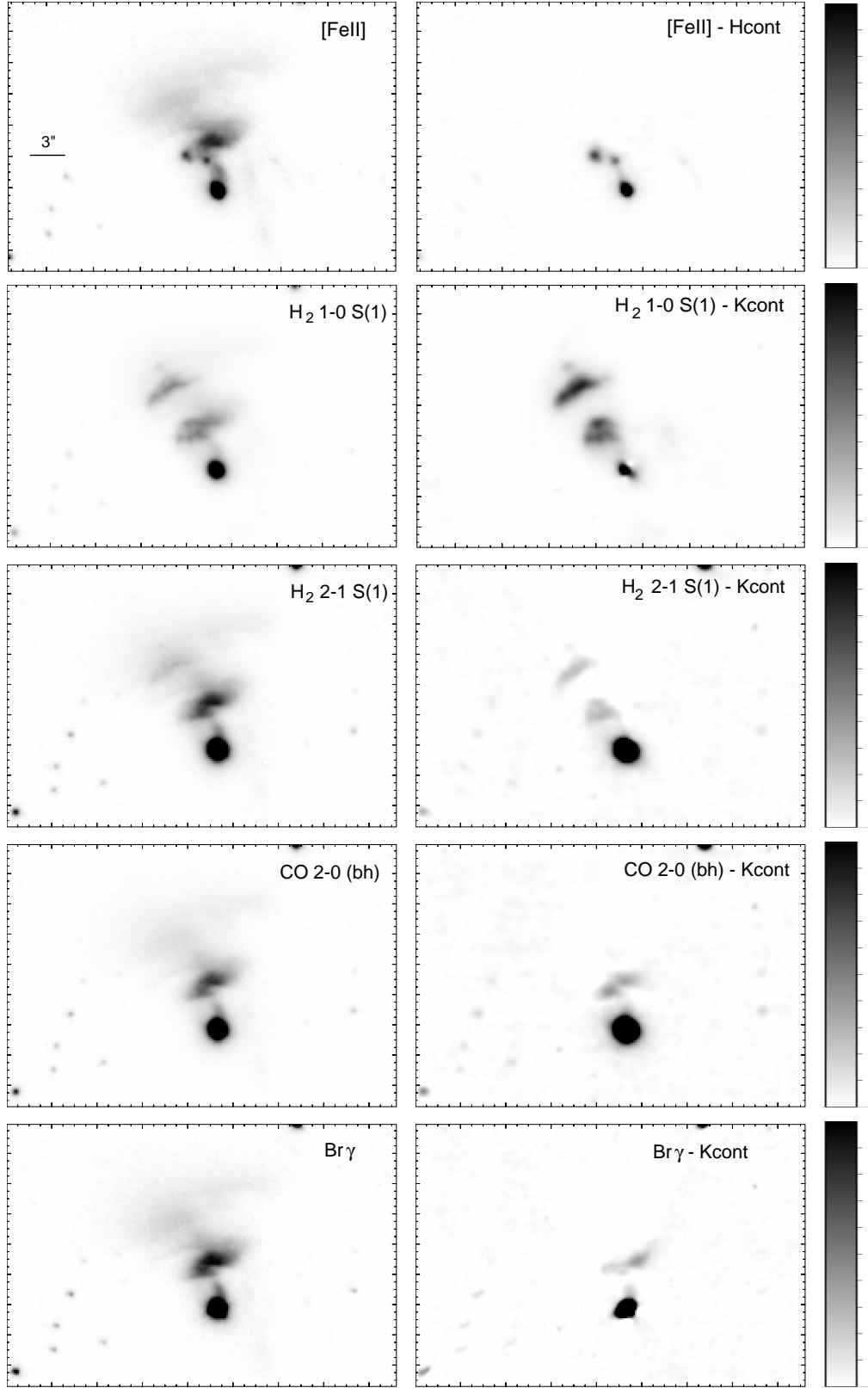


Fig. 4. Left panels: Narrow-band images centered at the indicated lines with continuum. Right panels: Narrow-band images centered at the indicated lines where the corresponding continuum was subtracted. The object nebular emission in all the subtracted images is above 5σ over the background. The white and black in the colorbars represent 0% and 100% of emission. The maximum values are (from top to bottom panel): 3, 35, 10, 15, and 10 ADU. All images were normalized to 1 sec.

close surroundings, is in H₂ 1-0 S(1). In the H₂ 1-0 S(1) continuum subtracted image several knots and filaments appear at

about 45'' (equivalent to 49.5 kAU in projection) around IRS towards the northwest and southwest, in perfect matching with the

Table 2. Offsets of emission-line features along the cone-like shape nebulosity determined from Gaussian fits to profiles shown in Fig. 5.

	Offset on sky (")	Offset on sky (AU)
[FeII]	1.78, 2.56	1958, 2816
H ₂ 1-0 S(1)	2.91, 6.05, 7.66	3200, 6655, 8426
Bry	2.63	2893
H ₂ 2-1 S(1)	2.74, 6.10, 7.64	3014, 6710, 8404
CO 2-0 (bh)	2.68	2948

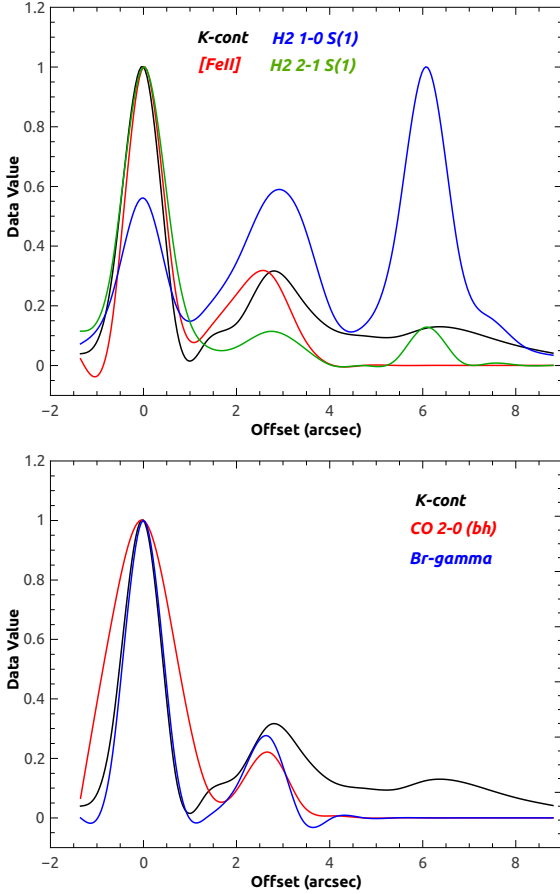


Fig. 5. Profiles of the line emission plotted along the axis of the cone-like shape nebulosity (the offset axis is measured in the plane of the sky). In the top panel profiles of [FeII], H₂ 1-0 S(1), and H₂ 2-1 S(1) are presented in red, blue, and green, respectively. In the bottom panel the profiles of CO 2-0 (bh) and Bry are presented in red and blue, respectively. In both panels, the continuum emission in *K*-band, observed with the *K*-cont filter (black), is included for comparison. The profiles are normalized to the peak emission.

distribution of the red and blueshifted molecular outflows discovered in Paper I. Figure 6 shows the H₂ 1-0 S(1) continuum subtracted emission with contours of the integrated ¹²CO J=3–2 line as presented in Paper I.

3.1. Proper motions

Following the precessing jet scenario and using two observations with temporal difference, it is possible to derive an estimation of the proper motions of some structure belonging to the cone-like

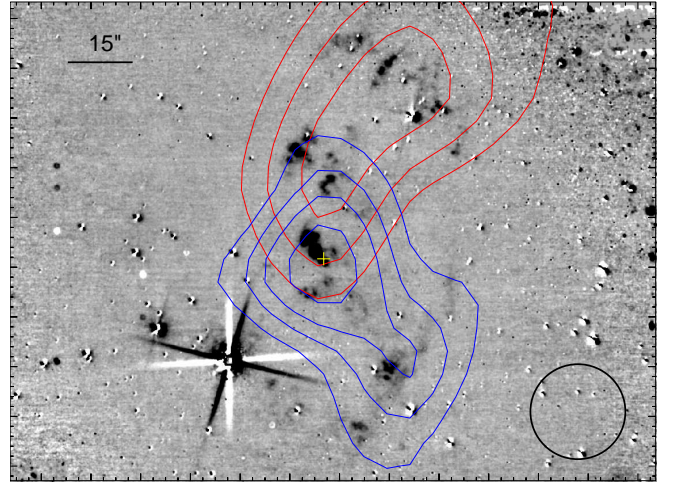


Fig. 6. H₂ 1-0 S(1) continuum subtracted emission with the ¹²CO J=3–2 contours superimposed, as presented in Paper I representing the red and blueshifted molecular outflows. The yellow cross is the IRS position and the beam-size of the ¹²CO observations is shown at the bottom right corner.

shape nebulosity. To do so we compare our *J*-band observations of the field, taken during August 2014, with the *J*-band image from the UKIDSS Survey taken during June 2005, providing a temporal interval of about 9 years. The angular resolutions are about 0.1 and 0.4 arcsec pix^{−1} for Gemini and UKIDSS, respectively. The astrometry of both images was checked based on the position of several point sources in the field and no evident offset was detected within the resolutions involved.

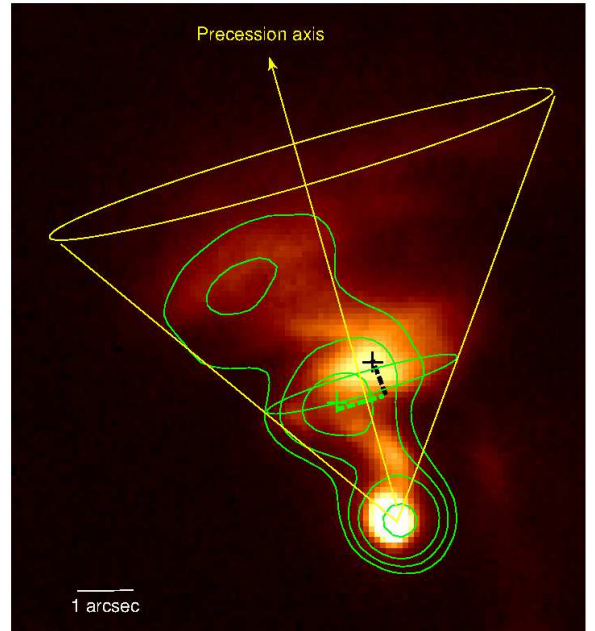


Fig. 7. Combination of the *J*-band emission obtained in two different epochs: the background image is from our observations obtained in 2014 while the green contours superimposed are from the UKIDSS Survey image obtained in 2005. The green and black crosses are the peak position at 2005 and 2014, respectively of the same clump-like feature related to the jet.

Figure 7 shows in the background the J -band emission obtained from our observations, and superimposed in green contours, the J -band emission from the UKIDSS Survey. Based on the morphology of the emission, we delineate the cone likely traced by the precessing jet (in yellow). The proper motion of the jet can be roughly characterized based on the assumption that the jet is moving onto the cone wall. In Fig. 7, the shift in the emission structure can be assessed by comparing a clump-like feature, whose peak position is indicated with a green cross for 2005, and with a black cross for 2014. Assuming that this feature is moving onto the cone wall, the spatial projected shift of 0.95 arcsec can be decomposed into two components. One component, perpendicular to the cone axis, related to the jet precession movement, of about 0.80 arcsec (green dashed line) and the other component, in vertical direction along the cone wall, associated with the ejection movement, of about 0.51 arcsec (black dashed line). Considering that the clump-like feature has taken about 9 years to cover the distance represented by the green dashed line, we estimate that it would take about 150 yr to cover the perimeter of the green circumference shown in Fig. 7 (precession period). Considering the other component of the proper motion represented by the black dashed line, we estimate an ejection velocity of about 200 km s^{-1} for the jet (a lower limit given possible projection effects not considered here), which is in good agreement with typical jets axial speeds from the literature ($100\text{--}400 \text{ km s}^{-1}$) (Mundt et al. 1990; Konigl & Pudritz 2000). Using these parameters and following Weigelt et al. (2006) and Smith & Rosen (2005), we can roughly analyze whether the jet precession period is slow or fast. In order to do that, it is necessary to compare the jet precession period with the outflow expansion time. This parameter is proportional to the jet dynamical time $t_j = r_j/v_j$ and the ratio of jet to ambient density, $\eta = \rho_j/\rho_a$, being r_j and v_j the initial jet radius and speed. Additionally, it is inversely proportional to $\sin(\theta)$, where θ is the half-angle of the precession cone. Using $v_j = 200 \text{ km s}^{-1}$ and $\theta = 35^\circ$, and assuming $r_j = 1.7 \times 10^{15} \text{ cm}$ and $\eta = 10$ (Smith & Rosen 2005), we obtain an outflow expansion timescale of about 50 yr. Thus, the fact that the jet precession period was estimated in 150 yr, three times larger than the outflow expansion timescale, suggests the presence of a slow-precessing jet. As Smith & Rosen (2005) point out, the slow-precessing jets generate helical flows, which is in agreement with the observed near-IR emission morphology.

4. Discussion

The cone-like shape nebulosity observed in the $JHKs$ broadbands points to the northeast of IRS opening in a wide-angle of about 70° . This near-IR emission likely arises from a cavity cleared in the circumstellar material and may be due to a combination of different emitting processes: radiation from the central protostar that is scattered at the inner walls of the cavity, emission from warm dust, and line emission from [FeII] and shock-excited H_2 , among other emission lines (e.g. Reipurth et al. 2000; Bik et al. 2005, 2006). Indeed, as shown in Fig. 4, some of these lines were detected. Additionally, the curved morphology of the jet-like feature and the twisted-shaped nebula, mainly observed in the J -band, strongly suggests the presence of a precessing jet. Models presented in Smith & Rosen (2005), pointed out that the dominant structure produced by a precessing jet is an inward-facing cone, and particularly, a slow-precessing jet leads to helical flows, generating a spiral shaped nebula. From our analysis of proper motions (see Sect. 3.1), we not only prove the existence of a precessing jet driven by IRS, but also that the precessing movement is slow (precession period = 150 yr),

giving strong observational support to the numerical models of Smith & Rosen (2005).

4.1. Emission-line features

For comparison, the observed emission lines are presented in colour-composed images in Fig. 8, which displays in the top panel, the continuum subtracted CO 2-0 (bh), H_2 1-0 S(1), and [FeII], in the middle panel the continuum subtracted Bry, H_2 1-0 S(1), and [FeII], and in the bottom panel the continuum subtracted CO 2-0 (bh) and Bry. It is known that the [FeII] emission traces the innermost part of jets that are accelerated near the driving source (Reipurth et al. 2000). The [FeII] is closely related to emission knots and shock fronts along the jet axis, tracing a high-velocity ($v \sim 50\text{--}200 \text{ km s}^{-1}$), hot ($T \sim 10^4 \text{ K}$), dense (electron densities $\sim 10^5 \text{ cm}^{-3}$), and partially-ionized region (Bally et al. 2007; Davis et al. 2011). The H_2 emission around YSOs usually delineates a slow ($v \sim 10\text{--}30 \text{ km s}^{-1}$), low-excitation, shocked molecular gas component ($T \sim 2 \times 10^3 \text{ K}$, $n \geq 10^3 \text{ cm}^{-3}$) (Bally et al. 2007; Davis et al. 2011). Besides of the collisional excitation mechanism, there is another possible mechanism to excite the H_2 emission that should be considered: the UV fluorescence. One way to discriminate between the collisional and radiative mechanisms is through the H_2 S(1) 1-0/2-1 ratio. In the collisional case, high ratios (about 10) are expected, while the radiative mechanism produces lower ratios (about 2) (e.g. Black & van Dishoeck 1987; Wolfire & Konigl 1991; Smith 1995). The H_2 S(1) 1-0/2-1 ratio analysis towards the features observed in the close surroundings of IRS shows that they are indeed produced by shocked gas, i.e. the H_2 emission is collisionally excited. Moreover, taking into account that in the closer arc-like feature the [FeII] and H_2 emissions are spatially coincident (see Fig. 8, upper and middle panels), we suggest that this feature may be produced by a J-shock, in which the [FeII] emission arises in regions where the shock velocity could be larger than 30 km s^{-1} , while the H_2 emission is originated in regions where the shock velocity is less than 25 km s^{-1} and the molecule is not dissociated (Hollenbach & McKee 1989; Smith 1994; Reipurth et al. 2000), or in the post-shock cooling region, where the molecules reform and radiate. Thus, even though a J-shock can be dissociative, emission from H_2 lines may be detected. In addition, it is important to keep in mind that iron can also be excited in C-shocks (Dionatos et al. 2013, 2014). On the other side, regions with H_2 emission without [FeII] can be explained by both, a nondissociative C-shock, or a less energetic J-shock (Hollenbach & McKee 1989; Dionatos et al. 2013, 2014). This is the case of the second arc-like feature in the surroundings of IRS and the H_2 1-0 S(1) features observed in a larger spatial scale shown in Fig. 6. As observed in the figure, these features perfectly correlate with the ^{12}CO outflows presented in Paper I, showing the presence of shocked molecular gas along them, and confirming its nature of molecular outflows.

The CO bandheads are excited in hot and very dense regions ($T > 2000 \text{ K}$ and $n > 10^{10} \text{ cm}^{-3}$), physical conditions that can be found in accretion disks (Scoville et al. 1983; Carr 1989; Bik & Thi 2004), neutral winds (Carr 1989), and funnel flows between the disk and the central source (Martin 1997). There is an intriguing issue regarding the Bry emission around IRS: on one side, Bry is excited at very high temperatures ($T \sim 10^4 \text{ K}$) and its emission usually spatially correlates with that of the CO 2-0 (bh) in YSO environments (Ilee et al. 2014 and references therein), which is not the case for IRS (see Fig. 8 bottom panel). Besides, according to Kumar et al. (2003), the Bry emission can arise in fast J-shocks within an envelope of thousands of AU sur-

rounding the young star. If it would be the case for IRS, then it is expected that the Br γ emission correlates with the [FeII] emission, which is also not the case for IRS (see Fig. 8 middle panel). We suggest that it is probable that the Br γ emission is associated with stellar wind (Kraus et al. 2008).

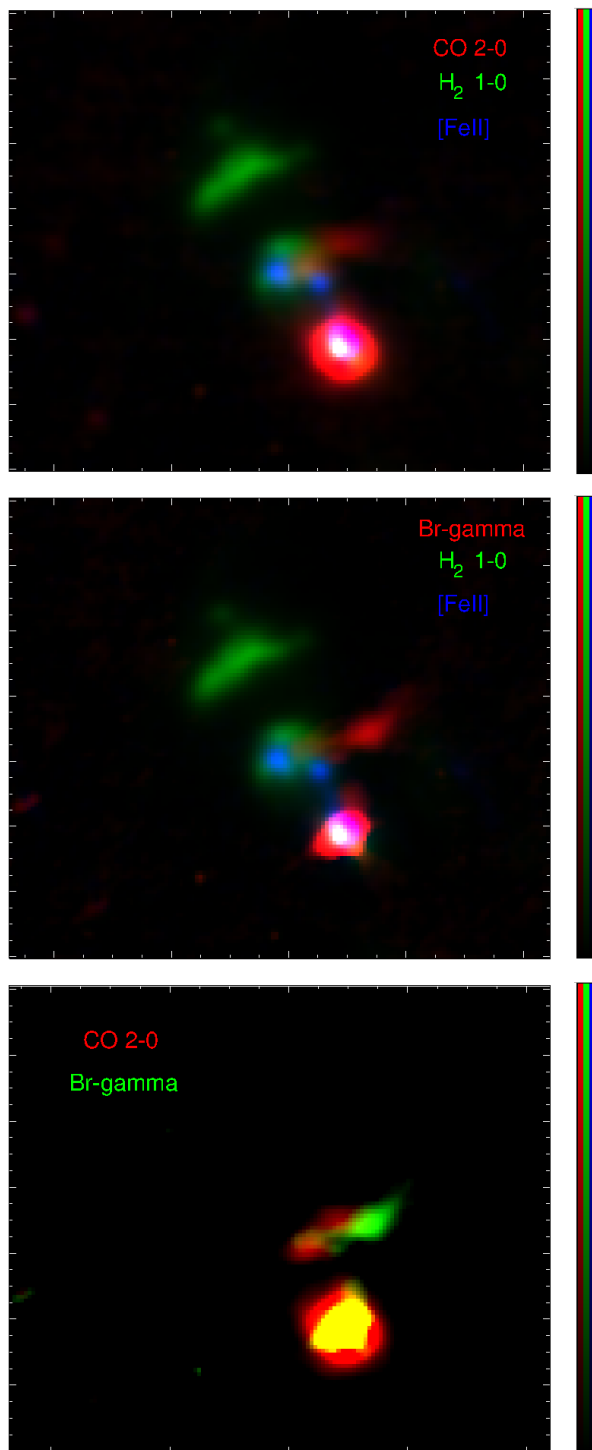


Fig. 8. Colour images composed with the continuum subtracted lines indicated in each panel. The black and the respective color in the colorbars represent 0% and 100% of emission. The maximum values are: 8, 50, and 2 ADU for red, green, blue, respectively in top and middle panels, and 5 ADU for red and green in the bottom panel. All images were normalized to 1 sec.

4.2. Considerations about the orientation of the observed circumstellar structures

We dedicate this section to discuss some aspects about the puzzling orientation of the molecular outflows detected in ^{12}CO J=3–2 and H_2 1–0 S(1) lines, compared with that of the jet, the arc-like features, and knots observed in the near-IR lines.

As shown in Paper I and reinforced in this study through the H_2 1–0 S(1) extended emission, which maps shocked molecular gas, the molecular outflows are indeed highly misaligned. The redshifted outflow points towards the northwest, while the blueshifted outflow points towards the southwest. Concerning the near-IR features in the close environment of IRS, as observed towards other similar sources (see Preibisch et al. 2003; Massi et al. 2004; Kraus et al. 2006; Weigelt et al. 2006; Paron et al. 2013) the nebula, with a cone shape and arc-like features, extends only to one side. In the mentioned studies, to justify this unidirectional asymmetry, it was proposed that the observed near-IR features should be related to a blueshifted jet with the redshifted counterpart not detected in the near-IR bands due to higher extinction. Indeed, when molecular outflows were observed through molecular rotational transitions, the nebula-like shape observed in the near-IR images matches the orientation and alignment of blueshifted molecular outflows. In the case presented here, the fact that the blueshifted molecular outflow points towards the southwest and the observed cone shape nebula with arc-like features towards the northeast is indeed puzzling. It may suggest that they are not related, or that probably there exist a complex relation, not evidenced in these images due to the large difference in the angular resolutions between the millimeter and near-IR data. One possibility could be that we are observing a not resolved system of YSOs. At the assumed distance of 1.1 kpc, the spatial resolution presented here is about 400 AU. It is known that a region of this size, or even smaller, can contain a binary system (Connelley et al. 2008). In an scenario with more than one YSO, it can be expected a complex (and so far unusual when comparing with low-mass YSO outflows studies) distribution of jets and molecular outflows, as it could be the case for IRS. In this way, the existence of a precessing jet may be explained through tidal interactions between companion stars.

Additionally, by inspecting the ^{12}CO J=3–2 distribution, it can be noticed that the peak of the blueshifted component coincides in projection with IRS. This shows that the ^{12}CO J=3–2 emission around IRS is predominantly blueshifted, which would relate the near-IR cone shape nebula to blueshifted gas. This agrees with an scenario with more than one YSO, where the blueshifted ^{12}CO J=3–2 peaking at IRS and the lobe extending towards the southwest are produced by different sources. Interferometric rotational lines CO observations are required to resolve the molecular outflows morphology.

5. Summary and concluding remarks

In Paper I we reported the presence of misaligned molecular outflows towards the intermediate-mass YSO UGPSJ185808.46+010041.8 (IRS) and based on public near-IR data we suggested the presence of a precessing jet. Aiming at studying in more detail this interesting source we present here the results derived from a new high-resolution image set obtained with Gemini-NIRI in the JHKs broad-bands and [FeII], H_2 1–0 (S1), Br γ , H_2 2–1 (S1), and CO 2–0 (bh) narrow-bands.

The near-IR imaging towards IRS, obtained with an spatial resolution of about 400 AU at the assumed distance of 1.1 kpc, strongly suggest a precessing jet. The observed cone-like shape

nebula composed by a twisted-shaped feature with two arc-like structures is one of the best images of this kind of objects presented up to date. These images give an important observational support to the models that point out that precessing jets generate this kind of near-IR features in massive YSOs. An analysis of proper motions based on our Gemini observations and UKIDSS data gives additional support to the precession scenario and allowed us to estimate a precession period of 150 yr, a jet axial speed of about 200 km^{-1} , and an outflow expansion timescale of about 50 yr. These parameters suggest the presence of a slow-precessing jet, which as shown by models presented in Smith & Rosen (2005), leads to helical flows in agreement with the structures observed in our near-IR images.

The analysis of the observed near-IR lines shows that the H_2 is collisionally excited, and the spatially coincide of the $[\text{FeII}]$ and H_2 emissions in the closer arc-like feature suggests that this region can be affected by a J-shock. However, it is important to keep in mind that iron can also be excited in C-shocks. The second arc-like feature presents H_2 emission without $[\text{FeII}]$, which could be explained by nondissociative C-shock or a less energetic J-shock, as is the case of the H_2 1-0 S(1) features observed in a larger spatial scale. In the H_2 1-0 S(1) continuum subtracted image, the only case in which near-IR emission was detected extending beyond the localized in the IRS close surroundings, several knots and filaments appear in perfect matching with the distribution of the molecular outflows discovered in Paper I, confirming shocked gas within the outflow lobes. Finally, we suggest that the Bry emission around IRS probably arises from stellar winds.

It is really puzzling the orientation of the molecular outflows (pointing the redshifted one towards the northwest and the blueshifted one towards the southwest), compared with the near-IR features (pointing towards the northeast). One possibility is a not resolved system of YSOs. The ^{12}CO J=3–2 emission around IRS is predominantly blueshifted, which suggests a relation between the near-IR cone shape nebula and the blueshifted gas. In this case, the blueshifted ^{12}CO J=3–2 peaking at IRS and the lobe extending towards the southwest can be produced by different sources. This scenario can explain the existence of a precessing jet through tidal interactions between companion stars. Interferometric rotational lines CO observations are required to resolve the molecular outflows morphology.

Acknowledgments

We thank the anonymous referee for her/his helpful comments and suggestions. The authors are very grateful to Gemini Staff for their dedication and helpful support in carrying out our observational programme. S.P. and M.O. are members of the *Carrera del Investigador Científico* of CONICET, Argentina. This work was partially supported by Argentina grants awarded by UBA (UBACyT), CONICET and ANPCYT.

References

Bally, J., Reipurth, B., & Davis, C. J. 2007, *Protostars and Planets V*, 215
 Bally, J., Walawender, J., Reipurth, B., & Megeath, S. T. 2009, *AJ*, 137, 3843
 Bally, J., Youngblood, A., & Ginsburg, A. 2012, *ApJ*, 756, 137
 Bik, A., Kaper, L., Hanson, M. M., & Smits, M. 2005, *A&A*, 440, 121
 Bik, A., Kaper, L., & Waters, L. B. F. M. 2006, *A&A*, 455, 561
 Bik, A. & Thi, W. F. 2004, *A&A*, 427, L13
 Black, J. H. & van Dishoeck, E. F. 1987, *ApJ*, 322, 412
 Carr, J. S. 1989, *ApJ*, 345, 522
 Ciardi, A. & Hennebelle, P. 2010, *MNRAS*, 409, L39
 Connelley, M. S., Reipurth, B., & Tokunaga, A. T. 2008, *AJ*, 135, 2496

Cutri, R. M., Skrutskie, M. F., van Dyk, S., et al. 2012, *VizieR Online Data Catalog*, 2281
 Davis, C. J., Cervantes, B., Nisini, B., et al. 2011, *A&A*, 528, A3
 Dionatos, O., Jørgensen, J. K., Green, J. D., et al. 2013, *A&A*, 558, A88
 Dionatos, O., Jørgensen, J. K., Teixeira, P. S., Güdel, M., & Bergin, E. 2014, *A&A*, 563, A28
 Erben, T., Schirmer, M., Dietrich, J. P., et al. 2005, *Astronomische Nachrichten*, 326, 432
 Hodapp, K. W., Jensen, J. B., Irwin, E. M., et al. 2003, *PASP*, 115, 1388
 Hollenbach, D. & McKee, C. F. 1989, *ApJ*, 342, 306
 Ilee, J. D., Fairlamb, J., Oudmaijer, R. D., et al. 2014, *MNRAS*, 445, 3723
 Konigl, A. & Pudritz, R. E. 2000, *Protostars and Planets IV*, 759
 Kraus, S., Balega, Y., Elitzur, M., et al. 2006, *A&A*, 455, 521
 Kraus, S., Hofmann, K.-H., Benisty, M., et al. 2008, *A&A*, 489, 1157
 Kumar, M. S. N., Fernandes, A. J. L., Hunter, T. R., Davis, C. J., & Kurtz, S. 2003, *A&A*, 412, 175
 Lefloch, B., Cernicharo, J., Reipurth, B., Pardo, J. R., & Neri, R. 2007, *ApJ*, 658, 498
 Lewis, B. T., Bate, M. R., & Price, D. J. 2015, *MNRAS*, 451, 288
 Lucas, P. W., Hoare, M. G., Longmore, A., et al. 2008, *MNRAS*, 391, 136
 Lumsden, S. L., Hoare, M. G., Urquhart, J. S., et al. 2013, *ApJS*, 208, 11
 Martin, S. C. 1997, *ApJ*, 478, L33
 Massi, F., Codella, C., & Brand, J. 2004, *A&A*, 419, 241
 McKee, C. F. & Ostriker, E. C. 2007, *ARA&A*, 45, 565
 Mundt, R., Buehrke, T., Solf, J., Ray, T. P., & Raga, A. C. 1990, *A&A*, 232, 37
 Paron, S., Fariña, C., & Ortega, M. E. 2013, *A&A*, 559, L2
 Paron, S., Ortega, M. E., Petriella, A., & Rubio, M. 2014, *A&A*, 567, A99
 Preibisch, T., Balega, Y. Y., Schertl, D., & Weigelt, G. 2003, *A&A*, 412, 735
 Reipurth, B. & Bally, J. 2001, *ARA&A*, 39, 403
 Reipurth, B., Yu, K. C., Heathcote, S., Bally, J., & Rodríguez, L. F. 2000, *AJ*, 120, 1449
 Reiter, M., Smith, N., Kiminki, M. M., Bally, J., & Anderson, J. 2015, *MNRAS*, 448, 3429
 Schirmer, M. 2013, *ApJS*, 209, 21
 Scoville, N., Kleinmann, S. G., Hall, D. N. B., & Ridgway, S. T. 1983, *ApJ*, 275, 201
 Smith, M. D. 1994, *MNRAS*, 266, 238
 Smith, M. D. 1995, *A&A*, 296, 789
 Smith, M. D. & Rosen, A. 2005, *MNRAS*, 357, 579
 Ukidss, C. 2012, *VizieR Online Data Catalog*, 2316, 0
 Weigelt, G., Beuther, H., Hofmann, K.-H., et al. 2006, *A&A*, 447, 655
 Wolfire, M. G. & Konigl, A. 1991, *ApJ*, 383, 205